Paper

Int'l J. of Aeronautical & Space Sci. 17(3), 324–331 (2016)
DOI: http://dx.doi.org/10.5139/IJASS.2016.17.3.324

IJASS
International Journal of Aeronautical and Space Sciences

An Experimental Study on the Characteristics of Rectangular Supersonic Jet on a Flat Plate

Ji-Young Kwak*

Department of Aerospace and Mechanical Engineering, Graduate School, Korea Aerospace University, Goyang City 10540, Republic of Korea

Yeol Lee**

School of Aerospace and Mechanical Engineering, Korea Aerospace University, Goyang City 10540, Republic of Korea

Abstract

The present study focuses on the characteristics of a supersonic jet flowing from a rectangular nozzle exit on a flat plate. Flow visualization techniques using schlieren and kerosene-lampblack tracing are utilized to investigate shock reflection structures and boundary-layer separations over a flat plate. Wall pressure measurements are also carried out to quantitatively analyze the flow structures. All observations are repeated for multiple jet flow boundary conditions by varying the flap length and nozzle pressure ratio. The experimental results show that the jet flow structures over the flat plate are highly three-dimensional with strong bleeding flows from the plate sides, and that they are sensitive to plate length and nozzle pressure ratio. A multi-component force measurement device is also utilized to observe the characteristics of the jet flow thrust vectoring over the plate. The maximum thrust deflection angle of the jet is about 8°, demonstrating the applicability of thrust vector control via a flat plate installed at the nozzle exit.

Key words: supersonic jet, rectangular nozzle, shock wave, flow separation

Nomenclature

H	Nozzle exit height, [mm]
L	Length of flat plate (or aft-deck), [mm]
M	Mach number
NPR	Nozzle pressure ratio
s	Gap distance between nozzle exit lip and plate surface, or backward step height [mm]
T	Resultant thrust, $T=\sqrt{T_x^2+T_z^2}$, [N]
T_z	Pitch thrust, [N]
T_x	Axial thrust, [N]
δ_p	resultant pitch thrust-vector angle, $\tan^{-1}(T_z/T_x)$, [deg]

1. Introduction

Many supersonic engine nozzles have employed non-axisymmetric geometries, including rectangular nozzles, to alleviate jet noise problems. Asymmetric nozzles have additional advantages such as easy airframe integration, which offers reduced drag and improved stealth capabilities in military applications. They are also a favorable choice to achieve thrust vectoring control. In the past several decades, many studies have been carried out to reveal the fundamental characteristics of supersonic jets from various rectangular nozzles [1-6]. For instance, in his study regarding the impact of rectangular nozzle aspect ratios on jet noise, Bridges [1] revealed that rectangular nozzles were able to reduce jet noise to a great degree than axisymmetric nozzles. Rice [2] also investigated the

* Graduate Student
** Professor, Corresponding author: ylee@kau.ac.kr

Received: April 8, 2016 Revised: July 1, 2016 Accepted: July 1, 2016

influence of nozzle exit geometry on the production of jet noise and mixing characteristics, showing that a double beveled C-D nozzle were able to reduce peak mixing noises by 4%.

Interactions between supersonic jet flows and flat plate (aft-deck) installed just downstream of the nozzle exit have drawn increasing attention. Seiner and Manning [7] studied supersonic jet-plate flows from a supersonic rectangular nozzle, and they showed that the gap distance between the nozzle exit and plate surface was an important parameter with respect to the jet screech tone. Research has also shown that jet noise characteristics are influenced by the flat plate (flap) length [8-9]. In addition, the turbulence characteristics of such jet flows and their impact on jet noise have also been studied both numerically and experimentally [10]. Most recently, Behrouzi and McGuirk [11] carried out an experimental study to reveal the behavior of an underexpanded rectangular supersonic jet flow with a very high aspect ratio near 7.4. They showed that the presence of an aft-deck at the nozzle exit had a strong effect on jet development and it reduced turbulence levels in the near fields of the jet. Multi-stream jets are also garnering attention due to their potential in reducing jet noise. Initially Papamoschou and Debiasi [12] demonstrated that the use of multiple streams enabled a reduction in jet noise. Many additional papers are currently being published to secure a better understanding of supersonic aft-deck flow structures in a three-stream engine concept (SERN) [13-14]

However, most of the literature on the subject has been focused only on the characteristics of turbulence jet mixing and jet noise. Relatively few studies have been published on the fundamental structures of supersonic jet flows over a nearby or parallel surface, and this is in spite of their importance in terms of fundamental fluid mechanics. The present study explores the flow field of a supersonic jet flowing from a rectangular nozzle exit with an extended flat plate (or aft-deck) of finite lengths and widths. Flow visualization techniques using schlieren and kerosene-lampblack tracing are utilized to investigate the shock reflection structures and boundary-layer separations over the flat plate. Wall pressure measurements are also carried out to quantitatively analyze the flow structures. Additionally a multi-component force measurement device is utilized to observe the thrust vectoring characteristics of the jet flow over the plate. All observations are repeated for various jet flow boundary conditions by varying the plate configuration and nozzle pressure ratio.

2. Experimental Facility and Instrumentation

2.1 Rectangular Nozzle and Flat Plate

Figure 1 shows a schematic for the nozzle configurations utilized in the present study. The nozzle chamber pressure is controlled by an electronic pressure controller (TESCOM, ER 3000SI-1), which maintains a constant pressure within about 3 % of a target value. The width and height of the rectangular sonic nozzle exit are 30 mm and 10 mm, respectively. The lip thickness of the nozzle exit is 1 mm. A flat plate is located just beneath the nozzle exit and spans the nozzle exit width. The plate is easily changeable and various plate lengths (L) ranging from 15 mm to 40 mm are tested. The gap distance (s) between the nozzle exit and the plate surface can be varied from 0 to 4 mm. A backward step thus forms naturally between the nozzle exit lip and the flap surface, and the upstream passage of the backward step is open to atmospheric pressure (refer Fig. 1). Static pressure taps are made on the flap surface to observe wall pressure variations on the plate during testing.

2.2 Flow Visualization and Pressure Measurement

The schlieren technique of the conventional Z-type configuration is utilized to qualitatively observe the jet flow field for various boundary conditions. The present schlieren setup includes two parabolic mirrors (diameter: 125 mm, focal length: 1,000 mm), two optical mirrors (diameter: 90 mm), and two light source types (LED-type: K-STL, Komi, spark-bulb type: LS-201, Komi). Schlieren visualization images are captured with digital cameras (CCD-type: CCE-B013-U, CMOS-type: SME-C012-U, Mightex). All digital visualization images are synchronized with other data such as the pressures and forces measured from load cells, and they are saved simultaneously on a PC via LabVIEW software. Surface flow visualizations utilizing the kerosene

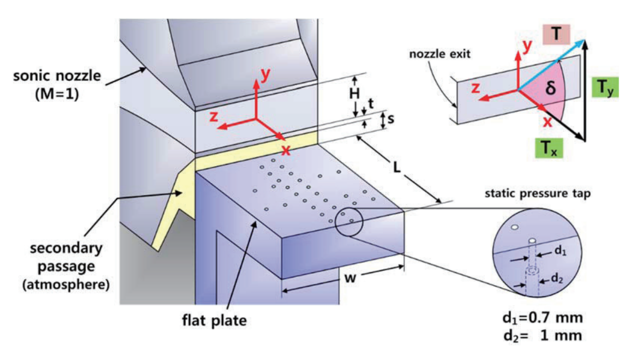

Fig. 1. Schematic diagram of the nozzle and plate assembly (not to scale)

and lampblack tracing technique are also conducted to investigate the surface flow patterns on the plate. The medium used for the technique is a combination of kerosene, lampblack and small amounts of a silicone oil. The pressures of the nozzle stagnation chamber and on the plate surface are measured using a pressure scanner (PSI 9116, Measurements Specialties) at a 60 Hz sampling rate, and they are also synchronized with other experimental data. The maximum measurement uncertainty of the pressure scanner is reported to be in the range of ±1.0 kPa.

2.3 Force Measurement

A salient feature of the supersonic jet flow on the plate is the occurrence of shock reflections and boundary-layer separations over the plate surface. The varying wall pressures that develop on the plate as a result of such complicated flow structures can introduce a net vertical force to act on the plate, *i.e.*, the downstream of the jet flow can be deflected upwards or downwards, depending on specific boundary conditions. In the present study, the nozzle block is assembled with a force measurement zig to investigate the applicability of the supersonic jet flow with the plate (flap) for thrust vectoring controls.

The present nozzle assembly and force measurement device use a vertical type design. The schematic diagram of the test chamber is shown in Fig. 2. A counter-balance weight is attached to align the axis of the center of gravity of the assembly to the load cells installed at the bottom of the nozzle block, thereby enabling the tare loads transmitted to the side load cells to be eliminated. Signals from the four load cells (CAS) in the test device are digitally recorded by a bridge-circuit module (NI 9237, NI) at a 1 kHz sampling rate. The pivot points of the two load cells measuring the side thrust are aligned to the nozzle exit plane, and two S-type load cells installed at the bottom center of the nozzle block measure the axial thrust.

Detailed calibrations and data analyses are performed to quantitatively estimate the measurement errors in the test device. The standard deviations and the repeatability

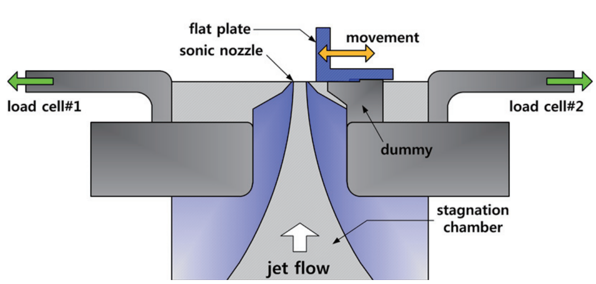

Fig. 2. Schematic diagram of the force measurement device

of each element in the coefficient matrix used in the thrust calculation procedure are less than 1 %. For all calibration loading conditions, the value of the interaction coefficients (the off-diagonal term of the coefficient matrix) is less than 1 % of the value of the direct coefficients (the diagonal term of the coefficient matrix). The overall maximum error of the present force measurement system is approximately in the range of 6-7 %. More detailed information, including the calibration procedure and the error analysis of the present test device, can be found in Reference [15].

3. Results and Discussion

3.1 Flow Structures for Various Plate Lengths and NPRs

All results described below are obtained for a sonic nozzle and constant nozzle stagnation temperature near 290 K during the tests. The schlieren images in Fig. 3 compare the jet flow structures over the plate for various plate lengths and *NPR*s. Here, *NPR* refers to the ratio of the nozzle stagnation pressure to the atmospheric pressure. The jet flow direction is left to right, and the white lines outline the plate. The plate surface tightly touches the nozzle exit lip in all cases, and thus the gap distance (s) is 0, if not mentioned otherwise.

Figure 3a is the reference case for comparison, in which no plate is installed at the nozzle exit. As shown in Figs. 3b to 3d, the plate length imposes a substantial influence on the highly compressible jet flow structures. As depicted in the third row of Fig. 3b, for an example, a strong oblique shock occurs at the end of the plate (deck shock). It is observed that the deck shock interacts with another shock just behind it, forming a lamda-shock structure. The jet flow is slightly displaced upward with a thick shear layer at the end of the plate. The shock structure in the jet flow field shows noticeable changes as the plate length increases. As shown in Fig. 3c, the oblique shock on the plate moves slightly downstream as the plate length increases to $L = 2.5H$. As depicted in the second row of Fig. 3c, an expansion wave (visible in the dark region in the schlieren image) forms at the end of the plate. The overall jet flow then deflects downward. As the plate length increases further up to $L = 4.0H$, the previous jet deflection patterns diminish, and the jet flow always deflects slightly upward, irrespective of *NPR* values. It is obvious that the jet deflection at the end of the plate is influenced by the changes of the shock cell pattern and the boundary-layer separation of the jet.

Although the schlieren images provide significant insight into the global flow structures, they are path integral of the density variations of the flow. Therefore, surface flow

DOI: http://dx.doi.org/10.5139/IJASS.2016.17.3.324

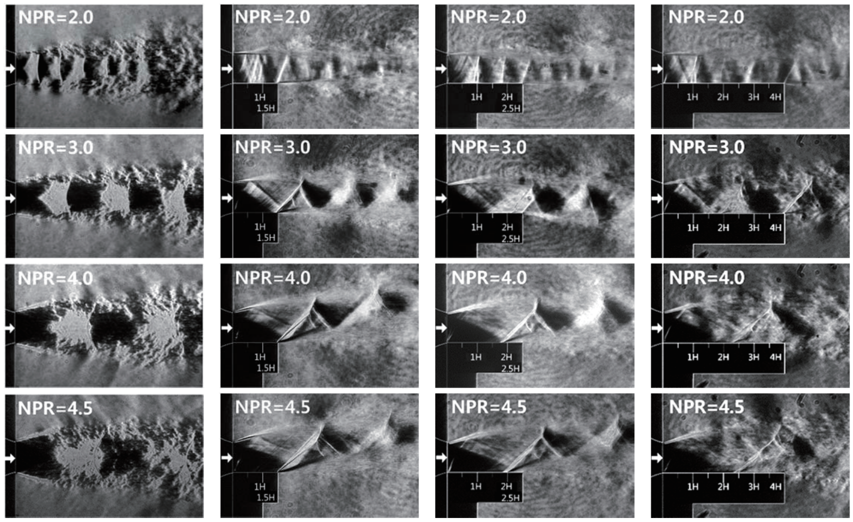

(a) $L = 0$ (b) $L = 1.5H$ (c) $L = 2.5H$ (d) $L = 4.0H$

Fig. 3. Schlieren images for various plate lengths and *NPR*s

visualizations on the plate surface are carried out using the kerosene-lampblack tracing technique. Fig. 4 presents several examples, in which the top view of the streaklines on the L=2.5H plate surface for various NPRs are represented. No appreciable streakline pattern has been noticed if the plate length is as short as L=1.5H. At a 300 kPa nozzle pressure (*NPR*=3.0), the compression waves reflected from the underexpanded upper jet boundary form a weak oblique shock on the plate as shown in Fig. 4a. A weak separation and reattachment of the jet boundary layer on the plate is shown with a thin parallel separation bubble merging to the centerline (visible in the bright layer in the streakline pattern). The jet boundary on the plate afterward is curved toward to the plate centerline, causing a strong spanwise inflow from the atmosphere. Strong flow separations are not noticed in this case, and the jet flow deflects downward at the end of the plate. As the *NPR* increases to 4.0, the overall shock structure shows a drastic change. The shock gets stronger and wider in the spanwise direction, and it moves slightly upstream to stand near x=1.75H. A pair of counter-rotating vortices symmetric to the centerline and separated from the plate is shown behind the shock. It is clearly shown that the jet core associated with the separation deflects upward at the end of the plate. The change in the overall shock structure between *NPR*=3.0 and *NPR*=4.0 is mainly attributed to the sudden change in the jet deflection at the end of the plate. Very little difference is observed in the overall surface streakline pattern for a higher *NPR* of 4.5 (see Fig. 4c).

Similarly, Fig. 5 shows the streaklines on the L=4.0H plate for various *NPR*s. The black dots in the figure denote

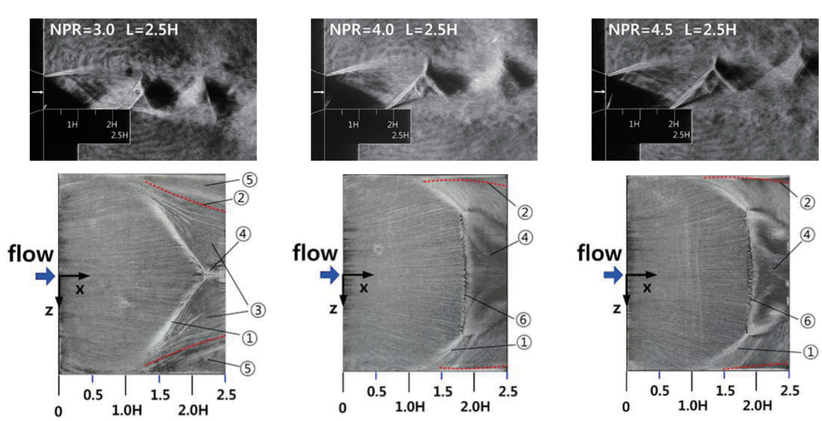

(a) *NPR*=3.0 (b) *NPR*=4.0 (c) *NPR*=4.5

① weak separation shock, ② jet boundary, ③ jet core, ④ counter-rotating vortices, ⑤ bleeding, ⑥ strong oblique shock

Fig. 4. Schlieren images and surface streaklines for various *NPR*s (L=2.5H, s=0)

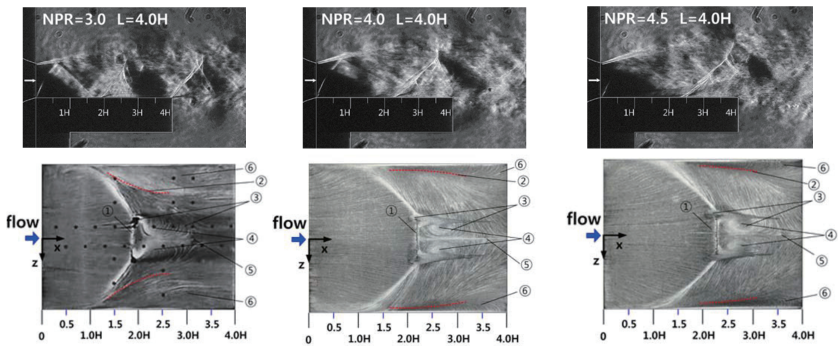

(a) *NPR*=3.0 (b) *NPR*=4.0 (c) *NPR*=4.5

① separation shock, ② jet boundary, ③ counter-rotating vortices, ④ focus, ⑤ saddle point, ⑥ bleeding

Fig. 5. Images of schlieren and surface streaklines for various *NPR*s (*L*=4.0*H*, *s*=0)

the static pressure holes drilled in the plate. When the *NPR* is equal to 3.0 with the longer plate length, a substantial change in the overall shock structure appears as compared to the previous shorter plate length (see Fig. 4a). The flow structure now includes a strong separation shock, a pair of counter-rotating vortices with two clear symmetric foci and a saddle point just behind the vortices. These features are similar to those seen in Figs. 4b and 4c. The jet boundary on the plate is again curved toward to the plate centerline, causing a strong spanwise inflow from both sides of the plate. As the *NPR* increases from 3.0 to 4.0, the streaklines from the nozzle exit show a more divergent pattern. In addition, the strong separation shock, vortices and saddle point move further downstream. The spanwise inflows from the plate sides, which were previously strong, become weaker, and the jet boundary extends to the sides of the plate. Very little difference is observed in the overall surface streakline pattern for the higher *NPR* of 4.5 (see Fig. 5c).

Strong spanwise atmospheric bleeding influences the overall flow structures, and it is apparent that the jet-plate flow is three-dimensional. To examine the effects of plate width on the three-dimensional structures on the jet-plate flow, a wider plate (the plate width = 10*H*) is installed at the nozzle exit instead of the previous plate (the plate width = 3*H*), and similar observations are carried out. No noticeable changes in the overall flow structures between the two cases are seen, except for a weak separation shock that moves slightly upstream in the case with the wider plate. Therefore, it is concluded that plate width does not significantly influence the overall jet flow structures on the plate, if it is larger than the nozzle width.

Wall static pressures along the centerline of the plate are measured for various *NPR*s and plate lengths to investigate the flow structures more quantitatively. The results are shown in Fig. 6. For $L = 2.5H$ as shown in Fig. 6a, the wall pressures initially decrease downstream due to the underexpanded jet conditions. As the *NPR* value increases, the wall pressure also increases. The pressures suddenly increase as the flow crosses the separation shock near $x/H = 1.75$, where x denotes the axial distance from the nozzle exit. The locations of the sudden increase in pressure match well with the shock locations in the surface streaklines shown in Fig. 4.

For $L = 4.0H$ as shown in Fig. 6b, the initial decrease of the wall pressure looks similar to that of the previous case shown in Fig. 6a. When the *NPR* is equal to 3.0, the pressure increases as the flow crosses the separation shock near $x/H = 1.75$. The pressure maintains a monotonous increase downstream through the vortex region, reaching to a maximum value up to a P/P_{atm} near

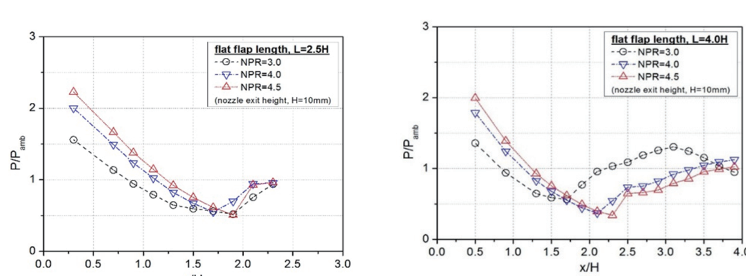

(a) $L = 2.5H$ (b) $L = 4.0H$

Fig. 6. Surface pressure distributions along the plate centerline for various *NPR*s (*s* =0)

DOI: http://dx.doi.org/10.5139/IJASS.2016.17.3.324

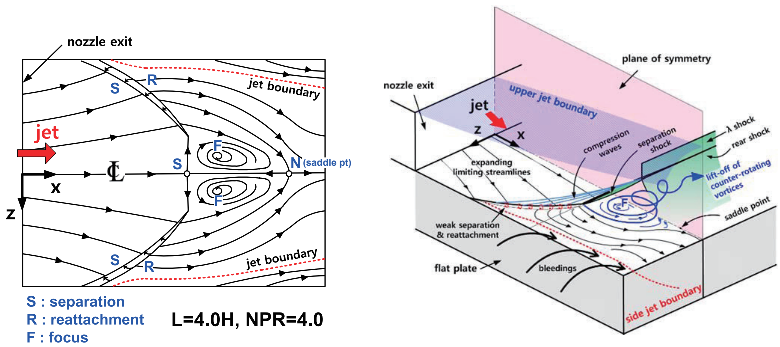

(a) surface flow model (b) 3-dimensional flow model

Fig. 7. Flow model of the jet flow over the flat plate (*NPR*=4.0, *L*=4.0*H*, *s*=0)

1.3 at x/H=3.1, and it then begins to decrease. The comparison of the surface streaklines shown in Fig. 5a with the present pressure variation clearly indicates that the location of the maximum pressure coincides with the saddle point just behind the vortex bubble. The phenomenon of the pressure decrease after the vortex bubble is presumed to be due to expansion waves reflected from the upper jet boundary. The expansion waves are visible in a dark region in the corresponding schlieren image in Fig. 5a. When the *NPR* is larger than 3.0, the pressure increase begins later in the axial direction, since the separation shock moves slightly downstream.

A flow model of the present jet-plate flow can be proposed to understand the three-dimensional shock structures and separation on the plate. By combining the schlieren images and the surface streaklines, the important features regarding the locations of the weak separation and reattachment of the jet boundary layer, saddle point, and forming vortices can be obtained, and the results are shown in Fig. 7. Fig. 7a shows the flow model of the limiting streamlines on the plate, and Fig. 7b shows the topological scheme for the case of *NPR*=4.0 and L =4.0H.

3.2 Jet Flow Thrust Vectoring

Complicated shock reflections and boundary-layer separation can cause a jet to deflect upwards or downwards, and they also determine the net vertical force on the plate. If a simple change of plate configuration, including plate length and/or gap distance, is able to change the jet deflection angle, this would enable efficient thrust vectoring control without the extra power consumption needed to blow/bleed the secondary control flows. Jet deflection characteristics are thus quantitatively investigated by utilizing the force measurement zig in the present study.

The measured deflection angles (δ_p) are shown in Fig. 8 for various plate configurations. The total uncertainty of the resultant deflection angles is estimated by the root sum square of the uncertainties of each T_x and T_z [15], and the uncertainty bars are put to each datum in the figures. As shown in Fig. 8a, if the jet is almost perfectly expanded (*NPR* = 2.0) and the gap distance (s) is set to 0, very little variation is observed in the jet deflection angle as a result of the change in plate length. If the *NPR* increases to 3.0, the change in the plate length introduces a substantial change in the pattern of the shock reflections and boundary-layer separations (refer Fig. 3). The jet deflects upwards (positive δ_p) or downwards (negative δ_p) according to the variation of plate length. However, the magnitude of the deflection angles is not that large. As the *NPR* increases further to 4.0 and 4.5, the deflection

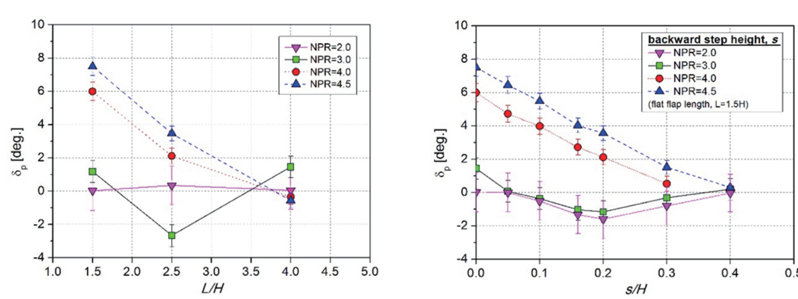

(a) plate length effects (*s*=0) (b) gap distance *s* effects (*L*=1.5*H*)

Fig. 8. Deflection angles for various plate and *NPR* configurations

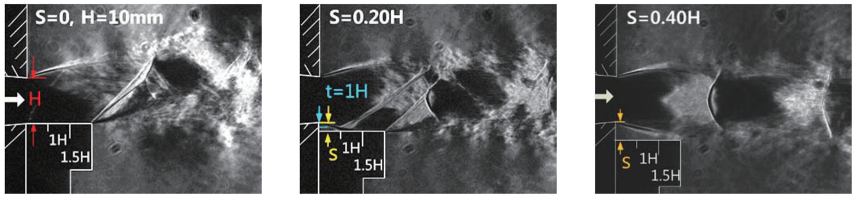

(a) $s = 0$ (b) $s = 0.2H$ (c) $s = 0.4H$

Fig. 9. Schlieren images for various gap distances (*NPR*=4.0, *L*=1.5*H*)

angle increases to the maximum value of 7.5° for the case in which L/H equals 1.5. When the *NPR* has such high values as 4.0 or 4.5, the deflection angle drops as the plate length increases. However, the jet always deflects upwards (positive δ_p values).

The effects of the gap distance between the nozzle exit lip and the plate surface (or backward step height) on the variation of the deflection angle are also observed as shown in Fig. 8b. The plate length is fixed as 1.5H here because the deflection angle is at its maximum in this case, and the angle becomes weaker as the plate length increases further, as already seen in Fig. 8a. Presently the secondary passage upstream of the backward step is open to atmospheric pressure. As shown in Fig. 8b, for low *NPR* values (2.0 and 3.0) the change in gap distance does not significantly influence on the jet deflection angle, and the angle remains almost flat near 0. When the *NPR* increases to 4.5, the maximum deflection angle is measured as high as 7.5° when s is equal to 0, and it decreases almost linearly as s increases. As depicted in Fig. 9, which shows schlieren images for various gap distances, the recirculating bubble just underneath the nozzle exit causes a separation shock at near the jet's reattachment location if s increases (see Fig. 9b). The effect of the backward facing step almost disappears if s increases up to about 0.4H and the jet flow expands freely without any interfering with the plate surface, as depicted in Fig. 9c.

Thrust losses associated with the present jet-plate flows are also quantitatively observed by estimating the resultant thrust ratio ($C_{fg,sys}$), which is defined as T/T_i. Here T is the measured resultant thrust (= $(T_x^2 + T_z^2)^{0.5}$) and T_i is the calculated isentropic axial thrust [16]. In the isentropic axial thrust calculation, the nozzle exit Mach number is assumed to be 1.0 since the jet flows are under-expanded for given *NPR* conditions. Therefore, the closer to 1.0 the value of the resultant thrust ratio is, the less the thrust loss is. Irrespective of the plate lengths and *NPR* values, the thrust losses due to the presence of the plate are found to be small, with a maximum value of about 3.0% ($C_{fg,sys} = 0.97$).

4. Conclusions

Flow visualizations and surface pressure/force measurements are utilized to investigate the structures of an underexpanded rectangular supersonic jet on a parallel plate. The effects of various nozzle pressure ratios and plate configurations on the shock reflections and boundary-layer separations on the plate are observed, and the following conclusions are drawn.

(1) A flow model with highly three-dimensional flows is obtained. A strong separation shock followed by a pair of counter-rotating vortices and bleeding flows from the plate sides are observed, and the shock and boundary-layer separation is attributed to the jet deflections downstream.

(2) For a specific conditon (*NPR* = 3.0), the jet deflection is able to be controlled in both upwards and downwards directions by changing the plate length. However, the window of the angle variation is narrow.

(3) The plate width does not significantly influence on the overall jet-plate flow structures, if the width is larger than the nozzle width.

(4) The change in the gap distance between the nozzle exit and the plate surface is able to introduce a linear variation of the jet deflection angle with a maximum positive angle of about 7.5°. The thrust losses associated with the jet-plate flows are found to be small, with a maximum value of about 3.0%

Acknowledgement

This research was supported by the Basic Science Research Program though the National Research Foundation of Korea (NRF) funded by the Ministry of Education, Science and Technology (2014-R1A1A2058320).

References

[1] Bridges, J. E., "Acoustic Measurements of Rectangular Nozzles with Bevel", *AIAA 2012-2252, 33rd AIAA Aeroacoustics*

Conference, Colorado Spring, CO, June 2012.

[2] Rice, E. J. and Raman, G., "Supersonics Jets from Bevelled Rectangular Nozzles", *NASA Technical Memorandum* 106403, 1993.

[3] Menon, N., *Analysis of Non-axisymmetric Underexpanded Jet Flow Fields*, Ph.D thesis, University of the Wotwatersrand, Johnnesburg, 2009.

[4] Seiner, J. M., "Fluid Dynamics and Noise Emission Associated with Supersonic Jets", *Studies in Turbulence*, Springer-Verlag, 1992.

[5] Zaman, K., "Spreading Characteristics of Compressible Jets from Nozzles of Various Geometries", *J. Fluid Mechanics*, Vol. 383, 1999, pp. 197-228.

[6] Alkislar, M. B., Krothapalli, A. and Louorenco, L. M., "Structure of a Screeching Rectangular Jet by a Stereoscopic Particle Image Velocimetry", *Journal of Fluid Mechanics*, Vol. 489, 2003, pp. 121-154.

[7] Seiner, J. M. and Manning, J. C., "Supersonic Jet Plume Interaction with a Flat Plate", *Proceedings of the international Power Lift Conference*, CA, USA, 1987.

[8] Bridges, J. E., "Noise from Aft Deck Exhaust Nozzle Differences in Experimental Embodiments", AIAA 2014-0876, *52th AIAA Aerospace Meeting*, Maryland, USA, Jan 2014.

[9] Zaman, K. B. M. Q., Fagan, A. F., Clem, M. M. and Brown, C. A., "Resonant Interaction of a Rectangular Jet with a Flat-plate", *AIAA 2014-0877, 52th AIAA Aerospace Meeting*, Maryland, Jan 2014.

[10] Ibrahim, M. K., Sawai, T., Obase, K., Mori, K. and Nakamura, Y., "Experimental Investigation of Screech Tone Characteristics of Jet Interaction with a Flat Plate", *AIAA Journal*, Vol. 47, No. 9, 2009, pp. 2031-2038.

[11] Behrouzi, P. and McGuirk, J. J., "Underexpanded Jet Development from a Rectangular Nozzle with Aft-deck", *AIAA Journal*, Vol. 53, No. 5, 2015, pp. 1287-1298.

[12] Papamoschou, D. and Debiasi, M., "Noise Measurements in Supersonic Jets Treated with the Mach Wave Elimination Method", *AIAA Journal*, Vol. 37, 1999, pp. 154-160.

[13] Magstadt, A. S., Berry, M. G., Coleman, T. J., Shea, P. R., Glauser, M. N., Ruscher, C. J., Gogineni, S. and Kiel, B. V., "A Near-field Investigation of a Supersonic, Multi-stream Jet: Locating Turbulence Mechanisms through Velocity and Density Measurements", *AIAA 2016-1639, 54th AIAA Aerospace Meeting*, CA, Jan 2016.

[14] Stack, C. M., Gaitonde, D. V., Agostini, L., Berry, M. G., Magstadt, A. S. and Glauser, M. N., "Numerical Investigation of a Supersonic Multistream Jet with Aft-Deck", *AIAA 2016-2058, 54th AIAA Aerospace Meeting*, CA, Jan 2016.

[15] Song, M. J., Chang, H. B., Cho, Y. H. and Lee, Y., "Development of the High-Accuracy Multi-Component Balance for Fluidic Thrust Vectoring Nozzle of UAV", *Journal of the Korean Society for Aeronautical and Space Sciences*, Vol. 41, No. 2, 2013, pp. 142-149.

[16] Flamm, J. D., Deere, K. A., Mason, M. L., Berrier, B. L. and Johnson, S. K., "Design Enhancements of the Two Dimensional, Dual Throat Fluidic Thrust Vectoring Nozzle Concept", *AIAA 2006-3701, 3rd AIAA Flow Control Conference*, CA, USA, June 2006.